Supplementary Information: Computational Discovery of Superior Vanadium Niobates Based Cathode Materials for Next-Generation All-Solid-State Lithium-Ion Battery Applications

Tanmoy Chakraborty,[1, a)] Bartomeu Monserrat,[2, 3] Alexandru Tănase,[1] Richard I. Walton,[1] and Bora Karasulu[1, b)]
[1)] *Department of Chemistry, University of Warwick, Coventry, CV4 7AL, United Kingdom*
[2)] *TCM Group, Cavendish Laboratory, University of Cambridge, J. J. Thomson Avenue, Cambridge CB3 0HE, United Kingdom*
[3)] *Department of Materials Science and Metallurgy, University of Cambridge, 27 Charles Babbage Road, Cambridge CB3 0FS, United Kingdom*

I. EXTENDED CONVEX HULL PLOT

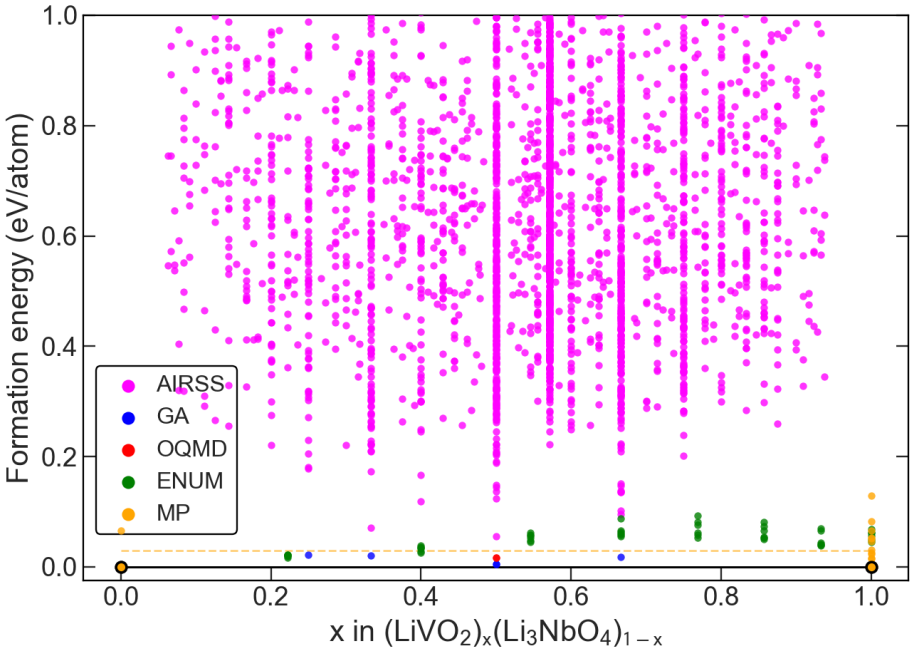

FIG. S1: Extended (up to 1 eV) Convex hull plot along the pseudobinary tieline of $LiVO_2$ and Li_3NbO_4

[a)] Electronic mail: tanmoy.chakraborty@warwick.ac.uk
[b)] Electronic mail: bora.karasulu@warwick.ac.uk

II. ELECTRONIC BAND STRUCTURE AND DOS OF THE END-MEMBERS

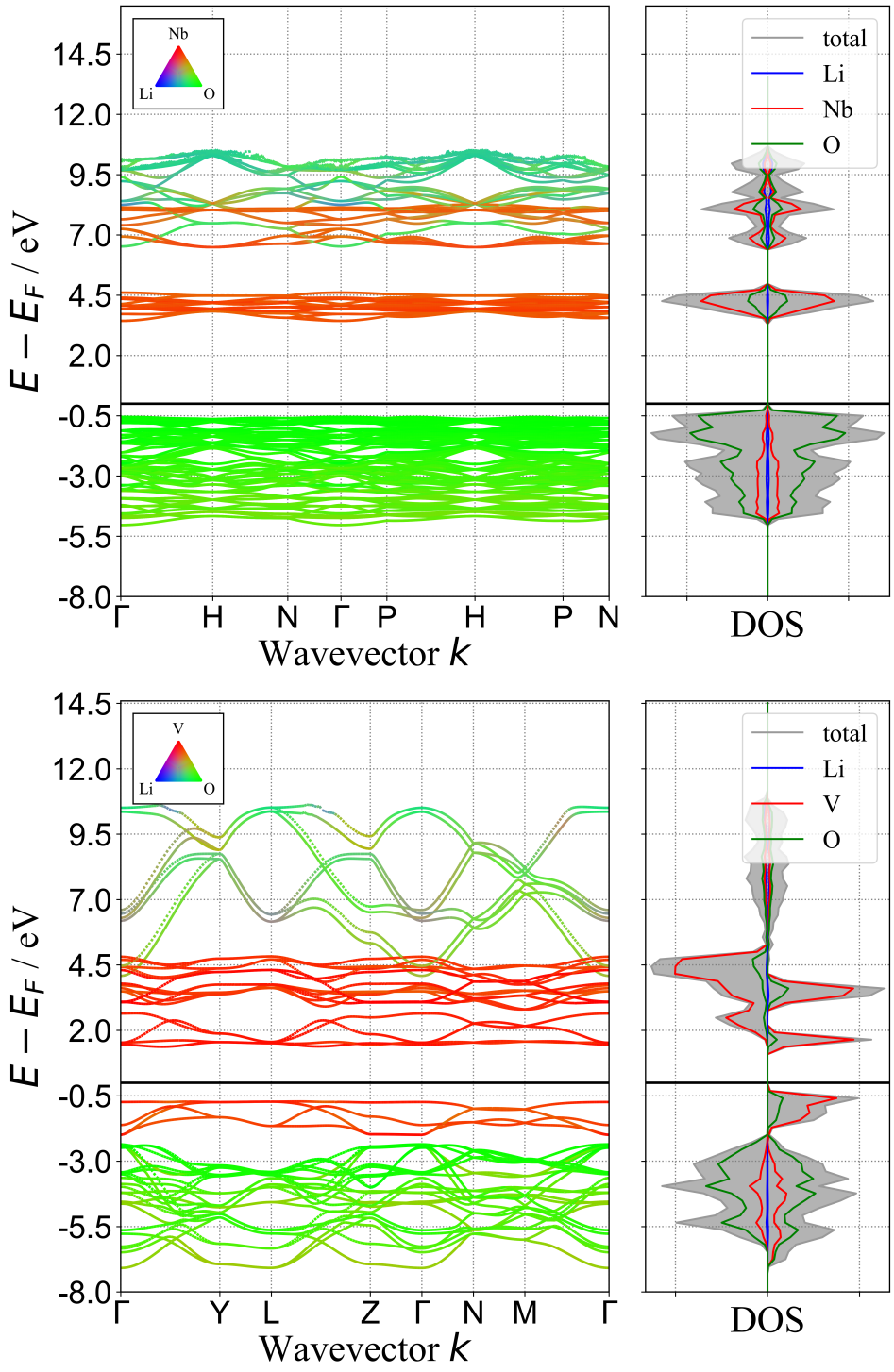

FIG. S2: Full electronic band structure and element-decomposed density of states of Li_3NbO_4 (upper panel) and $LiVO_2$ (lower panel).

III. ELASTIC TENSOR MATRIX ELEMENTS

A. Calculated elastic stiffness matrices (GPa) for $Li_{23}Nb_7V_2O_{32}$

$$\begin{bmatrix} 139.7432 & 73.6551 & 73.1212 & 0.0000 & 3.2134 & 0.0000 \\ 73.6551 & 158.3085 & 73.6575 & 0.0000 & 4.8760 & 0.0000 \\ 73.1212 & 73.6575 & 139.7465 & 0.0000 & 3.1790 & 0.0000 \\ 0.0000 & 0.0000 & 0.0000 & 82.0689 & 0.0000 & 3.3352 \\ 3.2134 & 4.8760 & 3.1790 & 0.0000 & 75.9082 & 0.0000 \\ 0.0000 & 0.0000 & 0.0000 & 3.3352 & 0.0000 & 82.0713 \end{bmatrix}$$

B. Calculated elastic stiffness matrices (GPa) for $Li_{10}Nb_3VO_{14}$

$$\begin{bmatrix} 194.4234 & 33.2563 & 58.3911 & -19.0745 & 11.3319 & 30.3011 \\ 33.2563 & 188.6667 & 56.6785 & -22.5136 & -0.4401 & -10.5771 \\ 58.3911 & 56.6785 & 246.7917 & -3.9165 & -10.7868 & 5.0173 \\ -19.0745 & -22.5136 & -3.9165 & 72.3946 & 14.3475 & 3.2532 \\ 11.3319 & -0.4401 & -10.7868 & 14.3475 & 70.4423 & -20.7564 \\ 30.3011 & -10.5771 & 5.0173 & 3.2532 & -20.7564 & 52.2394 \end{bmatrix}$$

C. Calculated elastic stiffness matrices (GPa) for $Li_7Nb_2VO_{10}$

$$\begin{bmatrix} 206.0873 & 28.6174 & 50.9770 & -16.6605 & 14.4313 & -20.5096 \\ 28.6174 & 142.6287 & 66.5688 & -14.3289 & -8.7348 & -60.3516 \\ 50.9770 & 66.5688 & 227.1967 & 1.1374 & -16.4642 & 5.8767 \\ -16.6605 & -14.3289 & 1.1374 & 78.1952 & -1.8415 & -19.4928 \\ 14.4313 & -8.7348 & -16.4642 & -1.8415 & 72.4890 & -20.8576 \\ -20.5096 & -60.3516 & 5.8767 & -19.4928 & -20.8576 & 51.2318 \end{bmatrix}$$

D. Calculated elastic stiffness matrices (GPa) for $Li_{11}Nb_3V_2O_{16}$

$$\begin{bmatrix} 137.3719 & 73.5767 & 64.1961 & 0.6240 & -0.3348 & -0.7452 \\ 73.5767 & 181.2518 & 77.5652 & 1.4714 & 1.2718 & -0.1313 \\ 64.1961 & 77.5652 & 147.5512 & 2.8896 & 3.1134 & 1.1987 \\ 0.6240 & 1.4714 & 2.8896 & 82.1752 & 2.4727 & 2.1740 \\ -0.3348 & 1.2718 & 3.1134 & 2.4727 & 74.2608 & 0.1463 \\ -0.7452 & -0.1313 & 1.1987 & 2.1740 & 0.1463 & 80.5213 \end{bmatrix}$$

E. Calculated elastic stiffness matrices (GPa) for Li_4NbVO_6

$$\begin{bmatrix} 232.0729 & 75.4580 & 51.7604 & 4.9748 & 15.7287 & -11.4873 \\ 75.4580 & 267.3645 & 75.0889 & 19.2620 & -2.6199 & 8.9683 \\ 51.7604 & 75.0889 & 157.1478 & 15.5074 & 44.1724 & 5.2564 \\ 4.9748 & 19.2620 & 15.5074 & 90.1656 & -7.5807 & -5.6583 \\ 15.7287 & -2.6199 & 44.1724 & -7.5807 & 68.3015 & 6.2763 \\ -11.4873 & 8.9683 & 5.2564 & -5.6583 & 6.2763 & 70.5198 \end{bmatrix}$$

F. Calculated elastic stiffness matrices (GPa) for $Li_5NbV_2O_8$

$$\begin{bmatrix} 295.7403 & 87.1525 & 79.7479 & 0.0000 & 0.3725 & 0.0000 \\ 87.1525 & 254.0902 & 54.6292 & 0.0000 & -1.0921 & 0.0000 \\ 79.7479 & 54.6292 & 110.5277 & 0.0000 & -3.9448 & 0.0000 \\ 0.0000 & 0.0000 & 0.0000 & 89.3691 & 0.0000 & -4.4797 \\ 0.3725 & -1.0921 & -3.9448 & 0.0000 & 88.1355 & 0.0000 \\ 0.0000 & 0.0000 & 0.0000 & -4.4797 & 0.0000 & 113.8277 \end{bmatrix}$$

IV. BVSE COMPUTED LI^+ MIGRATION PATHWAYS

A. $Li_{23}Nb_7V_2O_{32}$

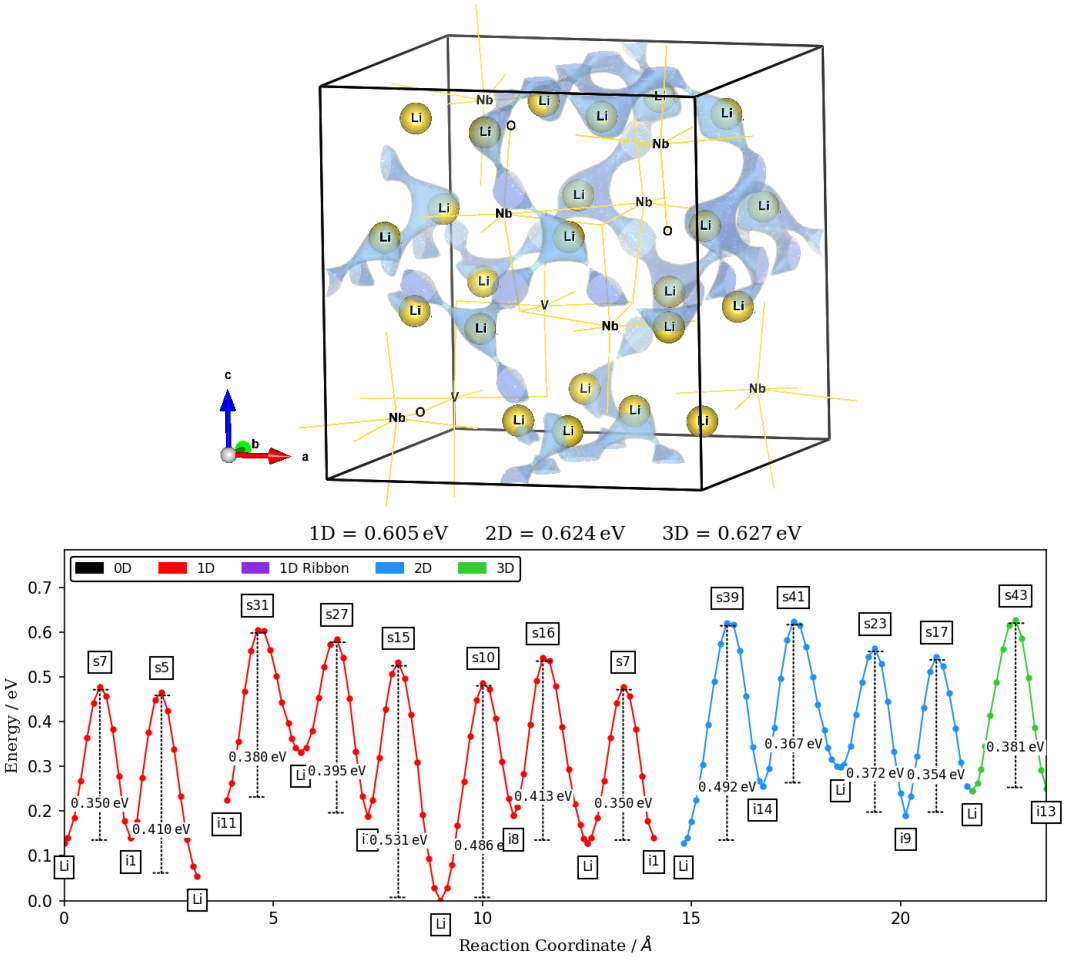

FIG. S3: BVSE computed Li^+ migration pathways and corresponding energy barriers for $Li_{23}Nb_7V_2O_{32}$ stoichiometry.

B. $Li_{10}Nb_3VO_{14}$

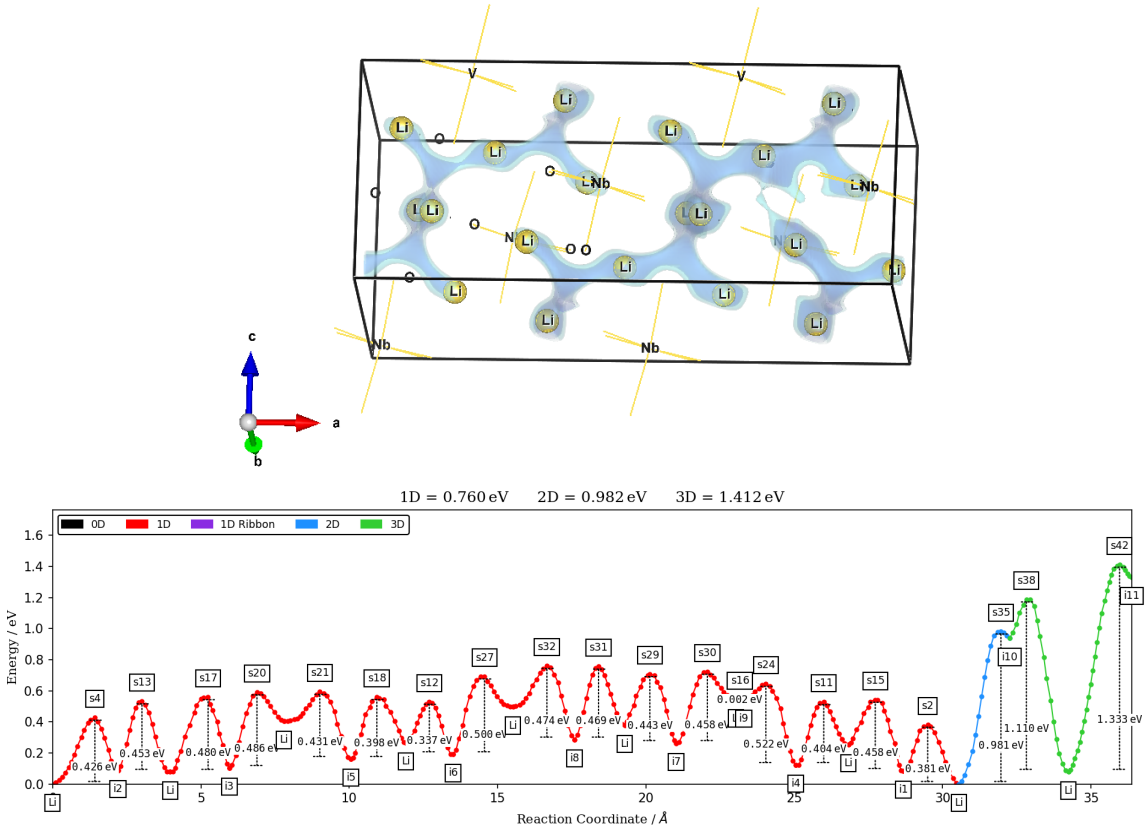

FIG. S4: BVSE computed Li^+ migration pathways and corresponding energy barriers for $Li_{10}Nb_3VO_{14}$ stoichiometry.

C. $Li_7Nb_2VO_{10}$

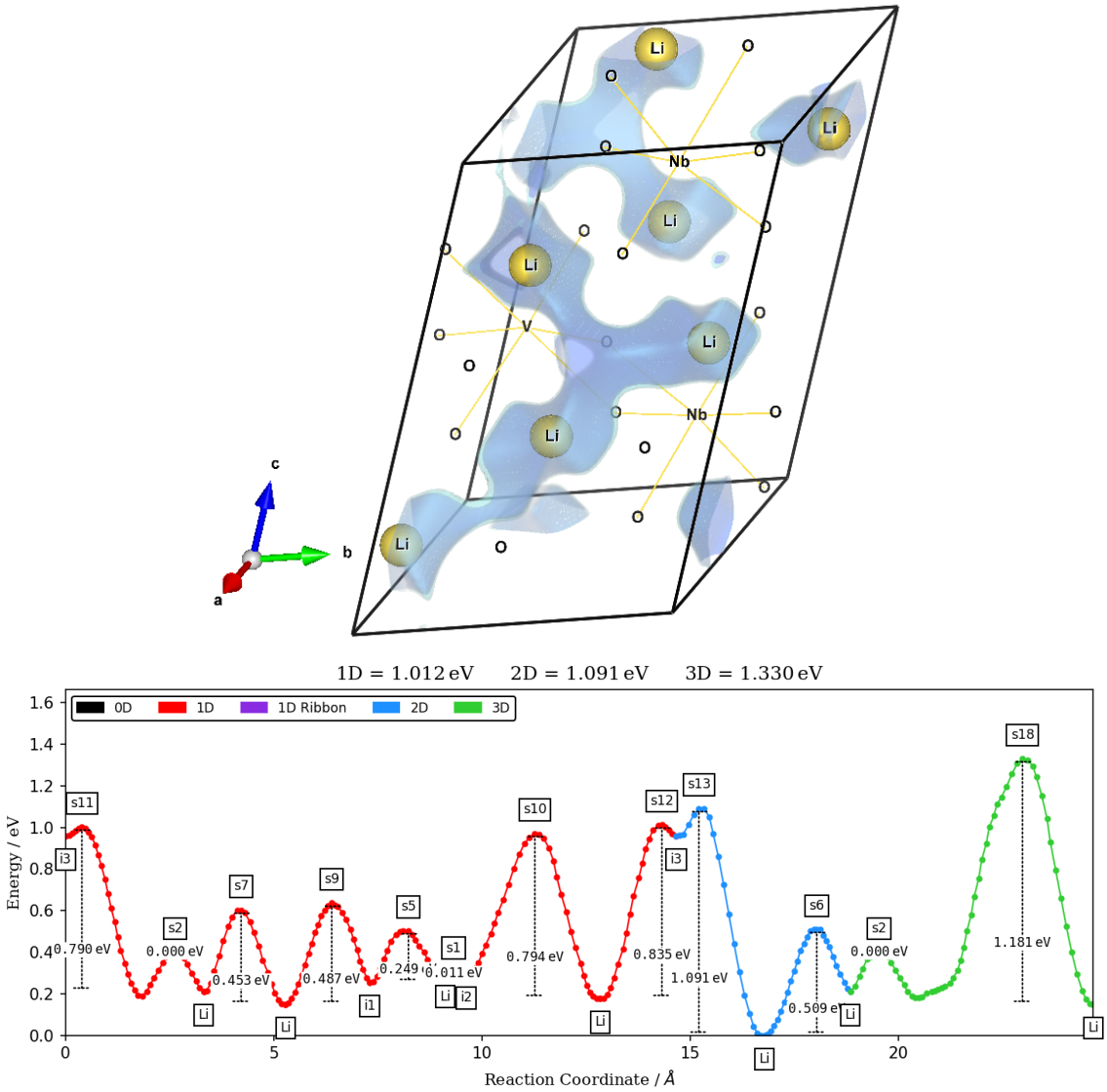

FIG. S5: BVSE computed Li^+ migration pathways and corresponding energy barriers for $Li_7Nb_2VO_{10}$ stoichiometry.

D. $Li_{11}Nb_3V_2O_{16}$

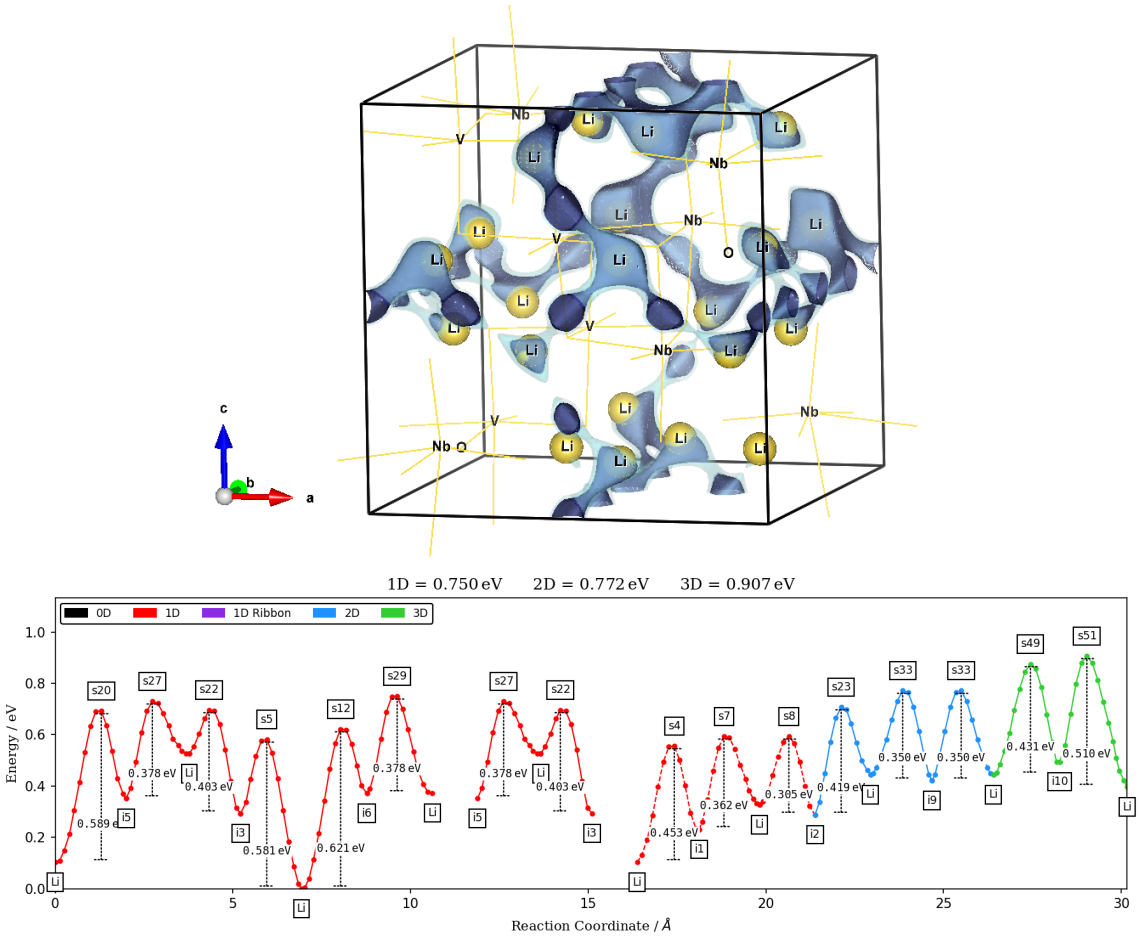

FIG. S6: BVSE computed Li^+ migration pathways and corresponding energy barriers for $Li_{11}Nb_3V_2O_{16}$ stoichiometry.

E. $Li_5NbV_2O_8$

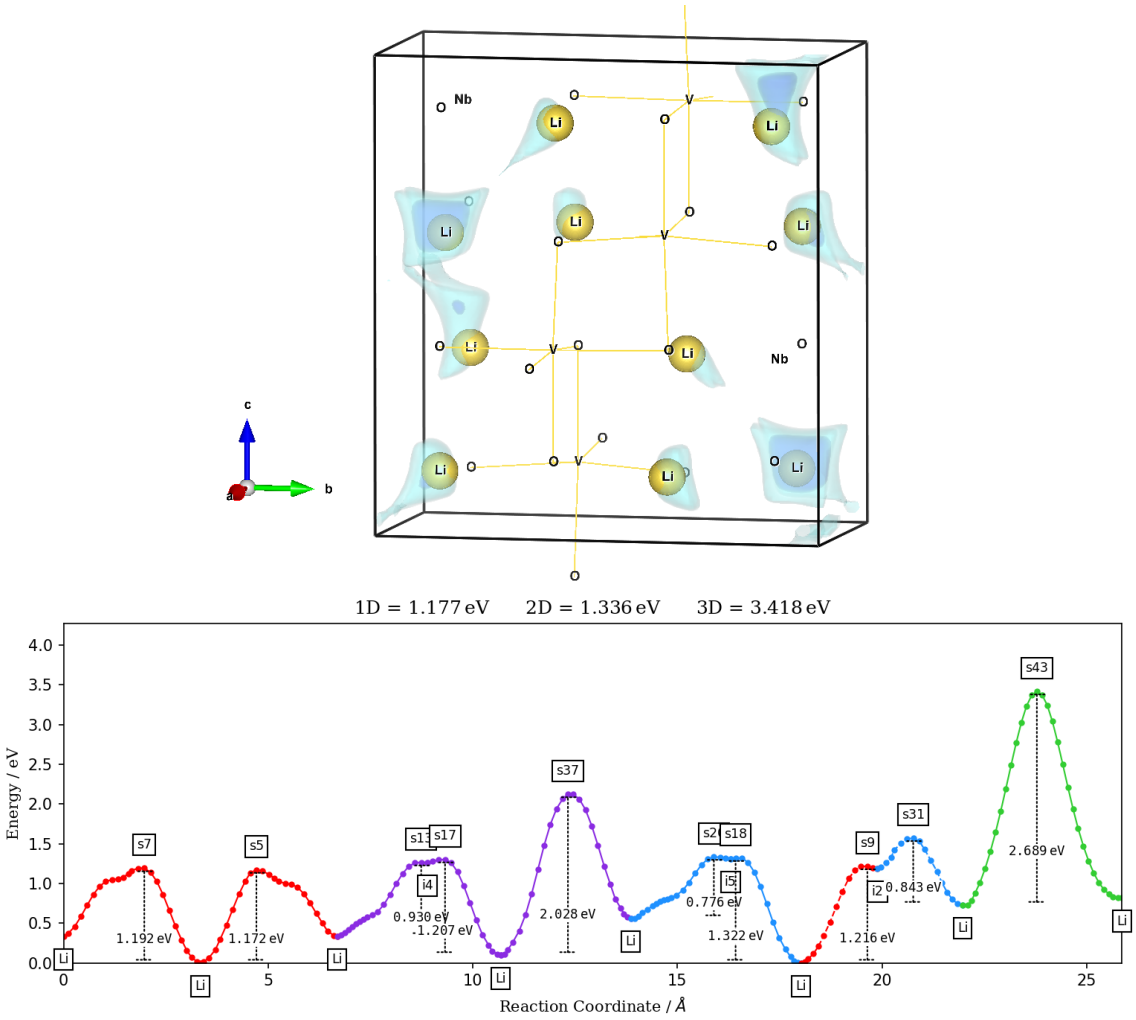

FIG. S7: BVSE computed Li^+ migration pathways and corresponding energy barriers for $Li_5NbV_2O_8$ stoichiometry.

V. HIGH-TEMPERATURE STABILITY

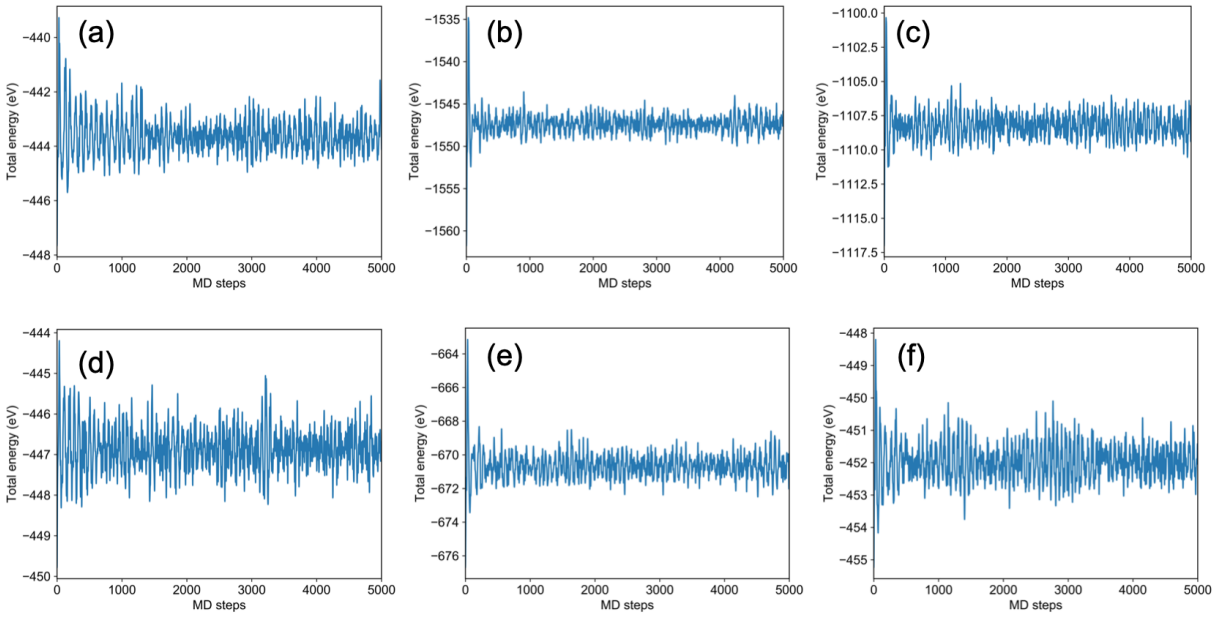

FIG. S8: Variation of total energy of (a) $Li_{23}Nb_7V_2O_{32}$ (b) $Li_{10}Nb_3VO_{14}$ (c) $Li_7Nb_2VO_{10}$ (d) $Li_{11}Nb_3V_2O_{16}$ (e) Li_4NbVO_6 and (f) $Li_5NbV_2O_8$ structures obtained from 600 K AIMD simulations during 10 ps run. For all cases, we see total energy remains constant around a mean value and thus further reflects the fact all the structures have excellent structural stability at high temperatures.

VI. MEAN SQUARED DISPLACEMENT PLOTS

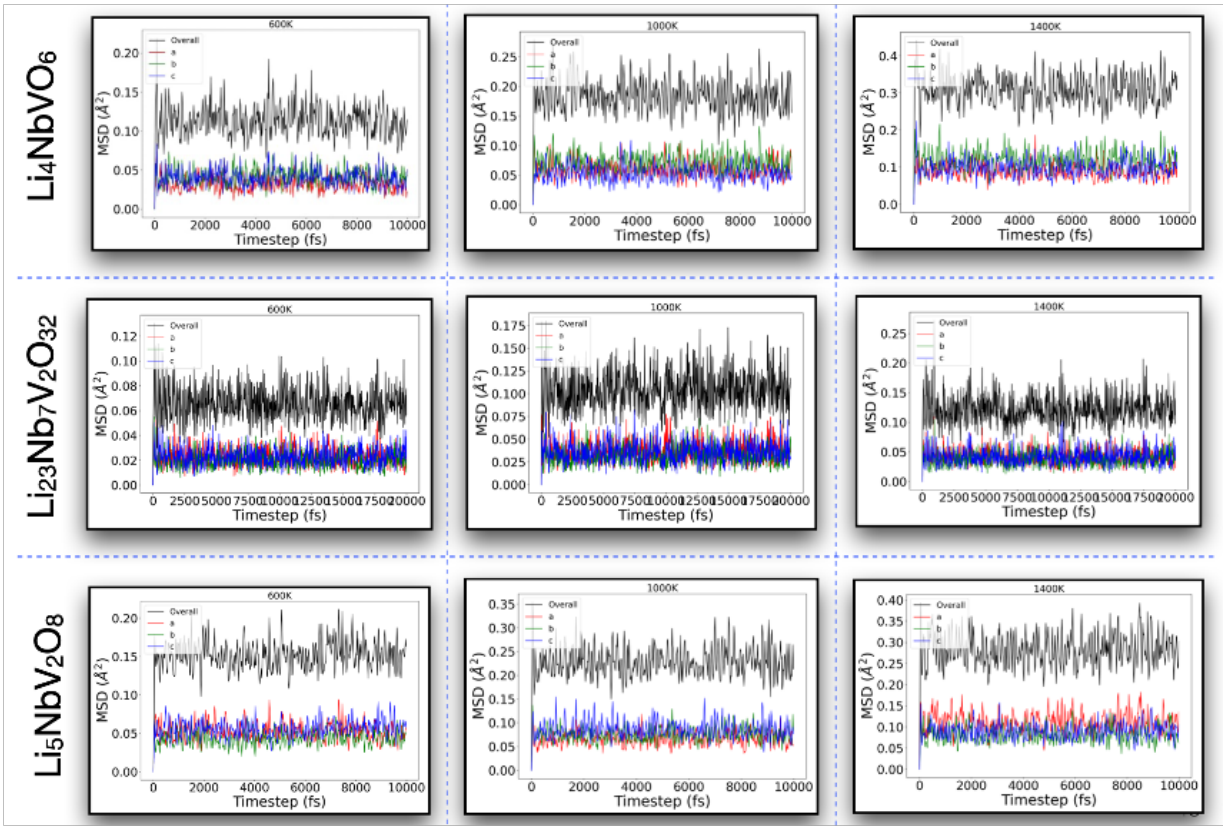

FIG. S9: Mean squared displacements plots of three novel stoichiometries at three different temperatures (600 K, 1000 K and 1400 K) extracted from AIMD simulations.